BJ www.biochemj.org

BJ Structure

Biochem. J. (2008) **416**, 317–326 (Printed in Great Britain) doi:10.1042/BJ20080632

Protein glycation *in vivo*: functional and structural effects on yeast enolase

Ricardo A. GOMES*, Luís M. A. OLIVEIRA*†, Mariana SILVA*, Carla ASCENSO†, Alexandre QUINTAS†, Gonçalo COSTA‡, Ana V. COELHO‡§, Marta SOUSA SILVA*, António E. N. FERREIRA*, Ana PONCES FREIRE* and Carlos CORDEIRO*[1]

*Centro de Química e Bioquímica, Departamento de Química e Bioquímica, Faculdade de Ciências da Universidade de Lisboa, Edifício C8, 1749-016 Lisboa, Portugal, †Laboratório de Patologias Neurodegenerativas, Instituto Superior de Ciências da Saúde Egas Moniz, 2829-511 Monte da Caparica, Portugal, ‡Laboratório de Espectrometria de Massa do Instituto de Tecnologia Química e Biológica, Universidade Nova de Lisboa, 2780-157 Oeiras, Portugal, and §Departamento de Química da Universidade de Évora, 7004-516 Évora, Portugal

Protein glycation is involved in structure and stability changes that impair protein functionality, which is associated with several human diseases, such as diabetes and amyloidotic neuropathies (Alzheimer's disease, Parkinson's disease and Andrade's syndrome). To understand the relationship of protein glycation with protein dysfunction, unfolding and β-fibre formation, numerous studies have been carried out *in vitro*. All of these previous experiments were conducted in non-physiological or pseudo-physiological conditions that bear little to no resemblance to what may happen in a living cell. *In vivo*, glycation occurs in a crowded and organized environment, where proteins are exposed to a steady-state of glycation agents, namely methylglyoxal, whereas *in vitro*, a bolus of a suitable glycation agent is added to diluted protein samples. In the present study, yeast was shown to be an ideal model to investigate glycation *in vivo* since it shows different glycation phenotypes and presents specific protein glycation targets. A comparison between *in vivo* glycated enolase and purified enolase glycated *in vitro* revealed marked differences. All effects regarding structure and stability changes were enhanced when the protein was glycated *in vitro*. The same applies to enzyme activity loss, dimer dissociation and unfolding. However, the major difference lies in the nature and location of specific advanced glycation end-products. *In vivo*, glycation appears to be a specific process, where the same residues are consistently modified in the same way, whereas *in vitro* several residues are modified with different advanced glycation end-products.

Key words: enolase, mass spectrometry (MS), methylglyoxal, methylglyoxal-derived advanced glycation end-product (MAGE), protein glycation, protein structure.

INTRODUCTION

Protein glycation is a non-enzymatic post-translational modification where arginine and lysine side-chain amino groups are irreversibly modified by carbonyl compounds, forming AGEs (advanced glycation end-products) [1,2]. Increased protein glycation is associated with several human pathologies such as diabetes mellitus and related clinical complications (retinopathy, nephropathy and diabetic vascular diseases) [3], uraemia [4], atherosclerosis [5], age-related disorders [3] and neurodegenerative diseases of the amyloid type [6–9]. Glycated proteins are present in β-amyloid and τ deposits of Alzheimer's disease [8,9], in Lewy inclusion bodies of α-synuclein in Parkinson's disease [10], in transthyretin amyloid deposits in familial amyloidotic polyneuropathy [11] and in amyloidotic lateral sclerosis [7]. In all of these amyloid pathologies, β-sheet fibril structure and the presence of AGEs are common features, suggesting a possible role for glycation in amyloid formation and pathogenesis. In diabetes mellitus and related clinical complications, D-glucose was considered to be the main glycation agent leading to irreversible changes in extracellular proteins [3]. However, several lines of evidence suggests that the increased glycation levels observed in several pathological conditions are not directly related to a higher D-glucose concentration, but to the increased concentrations of highly reactive low-molecular-mass carbonyl compounds, leading to what is described as carbonyl stress [4,12]. In fact, in several diseases where glycation products accumulate, glycaemia is normal [11]. Moreover, glycation is often found in intracellular proteins, as in Alzheimer's [9] and Parkinson's [10] diseases, where the D-glucose concentration is negligible. The dicarbonyl compound methylglyoxal is the most significant glycation agent *in vivo*, considering its high reactivity and continuous formation, mainly by the irreversible β-elimination of the phosphate group of dihydroxyacetone phosphate and D-glyceraldehyde-3-phosphate [13–15]. Albeit non-enzymatic, this is a physiological process that happens alongside glycolysis, hence methylglyoxal formation and protein glycation occur in all living cells. By reacting with the guanine group of arginine, methylglyoxal forms argpyrimidine, MG-H1 (hydroimidazolones) and THP (tetrahydropyrimidine) [1,2]. From its reactions with the ε-amino group of lysine, it forms CEL [N^{ε}-(carboxyethyl)lysine] and a MOLD (methylglyoxal-lysine dimer) [1,2]. These specific markers of protein glycation by methylglyoxal are globally known as MAGEs (methylglyoxal-derived AGEs). These MAGEs have been identified *in vivo* associated with diabetes [16] and in neurodegenerative disorders of the amyloid-type such as FAP (familial amyloidotic polyneuropathy) and ALS (amyotrophic lateral sclerosis) [7,11]. Previous evidence suggests that methylglyoxal and not other glycation agents specifically alter the function of several proteins [16a–16c]. One example is the specific modification of Arg^{188} of Hsp27 (heat-shock protein 27) with the formation of argpyrimidine, which is essential to the anti-apoptotic activity of this protein [17]. Moreover, glycation by methylglyoxal of small Hsps appears to be essential for its activation, suggesting a mechanism that

Abbreviations used: α-CHCA, α-cyano-4-hydroxicinamic acid; AGE, advanced glycation end-product; CEL, N^{ε}-(carboxyethyl)lysine; DHB, 2,5 dihydroxybenzoic acid; ESI, electrospray ionization; FTICR-MS, Fourier-transform ion cyclotron resonance MS; Hsp, heat-shock protein; MAGE, methylglyoxal-derived advanced glycation end-product; MALDI–TOF-MS, matrix-assisted laser-desorption ionization–time-of-flight MS; MG-H, hydroimidazolone; TFA, trifluororacetic acid; THP, tetrahydropyrimidine.

[1] To whom correspondence should be addressed (email caac@fc.ul.pt).

allows cells to detect and react to carbonyl and unfolding stress [17–20].

Intensive research has been conducted in the last decades whereby the effects of glycation on protein structure and function were investigated in conditions that bear no resemblance at all to what happens *in vivo* [21–24]. Use of concentrations of glycation agents up to the molar range is not uncommon. These studies are in sharp contrast with what happens inside living cells, where the methylglyoxal concentration is in the nano to micromolar range, whereas proteins are at a high concentration in a crowded and organized milieu [25]. Consequently, to investigate the effects of glycation on protein structure and function *in vivo*, cellular models must be sought where glycation conditions may be controlled. Yeast offers an ideal cell model to investigate glycation *in vivo*, now that glycation phenotypes and protein glycation targets have been uncovered [18,26,27]. Among these, enolase2p (2-phospho-D-glycerate hydrolase, EC 4.2.1.11), the main glycation target, shows a glycation-dependent enzyme activity loss [26].

In the present study, a detailed investigation of the effects of methylglyoxal-mediated glycation *in vivo* on the structure, thermal stability and enzyme activity of yeast enolase was performed. MAGE location and identification was made by a bottom-up approach, using MALDI–TOF-MS (matrix-assisted laser-desorption ionization–time-of-flight MS) and high mass accuracy FTICR-MS (Fourier-transform ion cyclotron resonance MS). Enolase2p was purified from *Saccharomyces cerevisiae* cells in glycation conditions (glycated *in vivo*) and in non-glycation conditions. The native enzyme was modified by methylglyoxal *in vitro*, in conditions often found in the literature. Striking differences between the effects of glycation *in vivo* and *in vitro* were observed. Among these, the heterogeneity of glycation *in vitro* is noteworthy, whereby different MAGEs are often formed at the same lysine or arginine residue, contrasting with the observation that *in vivo* a given MAGE is consistently found at the same amino acid residue.

EXPERIMENTAL

Chemicals and materials

Peptone, yeast extract and agar were from Difco, whereas D-glucose (microbiology grade), KCl and $MgSO_4$ were obtained from Merck. Ammonium sulfate, NaH_2PO_4, Na_2HPO_4, NaCl, NaF, DTT (dithiothreitol), iodoacetamide and TFA (trifluoroacetic acid) were from Sigma. Tris, 20 % (w/v) SDS and glycine were from Bio-Rad. EDTA was from BDH chemicals, whereas phosphoenolpyruvate, methylglyoxal 1,1-dimethyl acetal and DHB (2,5 dihydroxybenzoic acid) were from Fluka. Modified trypsin was from Promega. GELoader tips were from Eppendorf. POROS 10 R2 reversed-phase chromatography medium was from PerSeptive Biosystems. α-CHCA (α-cyano-4-hydroxicinamic acid), 3,5 dimethoxy-4-hydroxycinnamic acid (sinapinic acid), PepMix1 (MS peptide standards) and ProMix3 (MS protein standards) were obtained from LaserBiolabs. Amicon filters were purchased from Millipore. BSA protein digest was from Bruker Daltonics. Acetonitrile and methanol were HPLC-gradient grade and were obtained from Riedel de Häen; ultrapure water (type I) was produced in a Millipore Milli-Q system.

Methylglyoxal preparation

Methylglyoxal was prepared by acid hydrolysis of methylglyoxal 1,1-dimethylacetal as reported by Kellum et al. [28] and purified by fractional distillation under reduced pressure in a nitrogen atmosphere [29]. Once prepared, methylglyoxal solutions were standardized by enzyme assay with glyoxalase I and II, as described previously [30]. Purity was verified by HPLC and NMR analysis on a Bruker Advance 400.

Yeast strains and growth conditions

S. cerevisiae strains, Euroscarf collection (Frankfurt, Germany), were: BY4741 (genotype BY4741 *MATa*; *his3*Δ1; *leu2Δ0*; *met15Δ0*; *ura3Δ0*) and ΔGLO1 (isogenic to BY4741 with YML004c::KanMX4). Strains were kept in YPGlu agar slopes [0.5 % (w/v) yeast extract, 1 % (w/v) peptone, 2 % (w/v) agar and 2 % (w/v) D-glucose] at 4 °C and cultured in liquid YPGlu medium. To induce protein glycation, ΔGLO1 strain was cultured for 9 days to reach the stationary phase of growth [27]. The reference BY4741 strain was collected at the end of the exponential phase of growth (18 h).

Enolase purification

Native enolase was purified from BY4741 yeast cells at the end of the exponential phase of growth (18 h), whereas glycated enolase was purified from ΔGLO1 culture at the stationary phase (9 days), a condition where glycation was previously observed [27]. Purification was achieved by anion-exchange chromatography and size-exclusion chromatography after ammonium sulfate protein precipitation from crude extracts, based on a previously described method [31]. Cells were disrupted by sonication (5 cycles of 1 min at 100 W with 1 min cooling on ice). The extract was centrifuged at 40 000 ***g*** at 4 °C for 30 min to eliminate cell debris and adjusted to 50 % saturation of ammonium sulfate. Saturation was subsequently adjusted to 67 % by adding solid ammonium sulfate. After centrifugation at 40 000 ***g*** at 4 °C for 30 min, the supernatant was made 100 % saturated and centrifuged again. The pellet, containing enolase, was resuspended in 20 mM Tris/HCl (pH 8.2), containing 5 mM $MgSO_4$ and 1 mM EDTA. Sample was dialysed overnight at 4 °C against the same buffer to remove ammonium sulfate and loaded on to an ion-exchange chromatography DEAE-Sephadex A-50 column equilibrated with 20 mM Tris/HCl (pH 8.2), containing 5 mM $MgSO_4$ and 1 mM EDTA. Proteins were eluted with a linear NaCl gradient (0–0.5 M) at a flow rate of 1 ml $\cdot$ min^{-1} and the eluate was monitored at 280 nm. Protein-containing fractions were collected and probed by dot blot analysis using an anti-yeast enolase antibody (a gift from Dr H. M. Park, Department of Microbiology, Chungnam National University, Korea). Fractions containing enolase were collected, concentrated by ultrafiltration using Amicon filters and applied to a gel-filtration CM-Sephadex C-50 column, equilibrated with 50 mM NaH_2PO_4/Na_2HPO_4 buffer (pH 7.4) containing 150 mM NaCl, 5 mM $MgSO_4$ and 1 mM EDTA. Proteins were eluted with the same buffer at a flow rate of 1 ml $\cdot$ min^{-1}. Again, fractions containing enolase, probed by dot blot, were collected and combined. In the purification of glycated enolase, the protein fractions were also probed by dot blot with an anti-MAGE antibody (a gift from Dr. Ram Nagaraj, Case Western University, Cleveland, OH, U.S.A.). Enolase purity was evaluated by SDS/PAGE.

In vitro glycation of purified enolase by methylglyoxal

Purified native enolase (5 μM) was incubated with 10 mM methylglyoxal in 100 mM potassium phosphate buffer (pH 7.4) at 30 °C for 5 days in sterile conditions. Enolase concentration was determined spectrophotometrically ($\varepsilon_{280} = 0.89$ ml $\cdot$ mg^{-1} $\cdot$ cm^{-1}) [32] in a UV–visible Jasco V-530 spectrophotometer.

Western blot and HPLC analysis

Proteins (30 μg of protein per lane) were separated by SDS/PAGE in a Mini-protean 3 system (Bio-Rad), using a 12 % polyacrylamide separation gel and a 6 % polyacrylamide stacking gel. Proteins were transferred on to PVDF membranes (Hybond-P; Amersham Pharmacia Biotech), using the Mini Trans-Blot system (Bio-Rad). Transfer was performed with 39 mM glycine, 48 mM Tris, 0.0375 % SDS and 20 % (v/v) methanol. Prestained standard proteins (Bio-Rad) were also loaded on to the gel. Total proteins were stained with Ponceau S solution [0.5 % Ponceau S in 1 % (v/v) glacial acetic acid] to confirm protein transfer. For the dot blot assay, purified proteins were applied directly on to PVDF membranes previously activated with methanol and equilibrated with transfer buffer. The membranes were blocked overnight at 4 °C in 1 % (v/v) blocking solution (Roche) in TBS [50 mM Tris/HCl with 150 mM NaCl (pH 7.5)]. The anti-MAGE antibody was used diluted 1:5000 in 0.5 % blocking solution in TBS for 3 h, whereas the anti-enolase antibody was used diluted 1:10000 in the same conditions. Washes, secondary antibody and detection procedures were performed using the BM Chemiluminescence Western Blotting Kit (Roche) following the manufacturer's instructions.

Detection of glycation-induced fluorescence was monitored by reversed-phase HPLC on a Beckman–Coulter System Gold equipped with a Beckman–Coulter high-pressure binary gradient pump 126, a Beckman–Coulter 168-diode-array detector (1 nm resolution, 200–600 nm) and a fluorescence detector FP-2020 Plus (Jasco). The mobile phase consisted of 0.08 % TFA in type I water (solvent A) and 0.08 % TFA in acetonitrile (solvent B), and the elution gradient program was: 10–80 % solvent B in 30 min and 80–10 % solvent B in 10 min. Separation was achieved on a reversed-phase analytical column (LiChrospher 100 Merck RP-18, 5 μm) at a flow rate of 1 ml $\cdot$ min^{-1}. Eluting species were monitored by the fluorescence signal at $\lambda_{em}/\lambda_{exc}$ of 320/385 nm, characteristic of argpyrimidine.

MS analysis

MALDI–TOF mass spectra were acquired in a Voyager-DE STR MALDI–TOF (Applied Biosystems). FTICR-MS mass spectra were obtained in a Bruker Apex Ultra with a 7 Tesla magnet (Bruker Daltonics). For intact protein mass measurement, sinapinic acid (20 mg $\cdot$ ml^{-1}) prepared in 70 % (v/v) acetonitrile with 0.1 % TFA was used as the matrix, and MALDI–TOF spectra were obtained in positive linear mode. To identify the purified proteins and assign the glycated amino acid residues, a peptide mass fingerprint was performed. Protein bands were excised and subjected to reduction, alkylation and digestion with sequencing-grade modified trypsin in gel, according to Pandey et al. [33]. The peptide mixture was purified, concentrated by R2 pore microcolumns [34] and eluted directly to the MALDI target plate with 0.8 μl of recrystallized matrix α-CHCA (10 mg $\cdot$ ml^{-1}) prepared in 70 % (v/v) acetonitrile with 0.1 % TFA. Monoisotopic peptide masses were used to search for homologies and protein identification with Peptide Mass Fingerprint of Mascot (http://www.matrixscience.com). The identification of glycated amino acid residues was performed as described previously [26]. Briefly, a glycated enolase peptide should have a miscleavage associated with the defined mass increment of a specific MAGE. Moreover, an arginine modification should have a miscleavage in an arginine residue and the same holds true for lysine modifications [26]. The analysis of glycated peptides was also performed by FTICR-MS. In this case, besides in-gel digestion, proteins were hydrolysed in-solution, essentially as described [35]. The resulting peptide mixture was also purified using PerfectPure C-18 tips (Eppendorf) and diluted in 50 % (v/v) methanol with 1 % (v/v) formic acid for ESI (electrospray ionization)–FTICR-MS analysis. The peptide mixture was analysed by MALDI–FTICR-MS, using DHB matrix [10 mg $\cdot$ ml^{-1} prepared in 70 % (w/v) acetonitrile with 0.1 % TFA] in an Anchorchip MALDI target (Bruker Daltonics).

Structure and stability analysis

Structural analysis was performed by CD spectroscopy and gel-filtration chromatography. Prior to CD analysis, individual protein species were separated by gel filtration on an analytical column (Amersham-Pharmacia Superdex™ 75 10/300 GL) with 10 mM phosphate buffer (pH 7) containing 100 mM NaF as the mobile phase at a flow rate of 0.4 ml $\cdot$ min^{-1} (LKB Bromma 2150 isocratic pump with a UV detector JASCO 2075). Eluting peaks were monitored at 280 nm and individual protein fractions were collected for further analysis.

Secondary structure analysis was performed by far-UV (185–240 nm) CD in a Jasco J810 spectropolarimeter at 25 °C (Julabo F25 temperature control unit) with a 0.1 cm path length. CD spectra were deconvoluted using the CDSSTR algorithm [36] on Dichroweb (http://www.cryst.bbk.ac.uk/cdweb/html/home.html) [37,38]. Molar ellipticity was calculated on the basis of a mean residue mass of 107.13 Da. All spectra were solvent baseline-corrected. Conformational stability measurements were performed by thermal-induced protein unfolding. CD denaturation curves were constructed by raising the temperature from 20 to 85 °C and measuring the ellipticity at 222 nm. The T_m value (temperature at which 50 % of denaturation occurs) of native and glycated enolase was calculated as previously described [39].

Enolase activity assay

Enolase activity was determined at 30 °C in a 1.5 ml reaction volume, on a Beckman DU-7400 diode array spectrophotometer, with temperature control and magnetic stirring, essential to maintain isotropic conditions during the assay. Enolase activity was followed by measuring phosphoenolpyruvate consumption at 240 nm and its concentration was calculated using $\varepsilon = 1.42$ mM^{-1} $\cdot$ cm^{-1} (the present study). The reaction mixture, containing 50 mM Tris/HCl (pH 7.4), 100 mM KCl, 1 mM $MgSO_4$, 0.01 mM EDTA and a known amount of protein, was pre-incubated for 10 min and the reaction was started by the addition of phosphoenolpyruvate.

Protein structure

The enolase dimer structure was represented by PDB entry 1EBH. Molecular graphics images were produced using the UCSF Chimera package from the Resource for Biocomputing, Visualization, and Informatics at the University of California, San Francisco, CA, U.S.A. [supported by NIH (National Institutes of Health) P41 RR-01081] [40]. Relative solvent surface accessibility was calculated according to Gerstein [41].

RESULTS

Characterization of enolase glycation by MS

Native enolase was purified from the BY4741 reference strain at the end of the exponential phase of growth and glycated *in vitro* by incubation with 10 mM methylglyoxal in potassium phosphate buffer, the most common glycation condition [42–44]. Purified native enolase also served as a control for enzyme activity, secondary structure composition and thermal stability. *In vivo*-glycated enolase was purified from the ΔGLO1

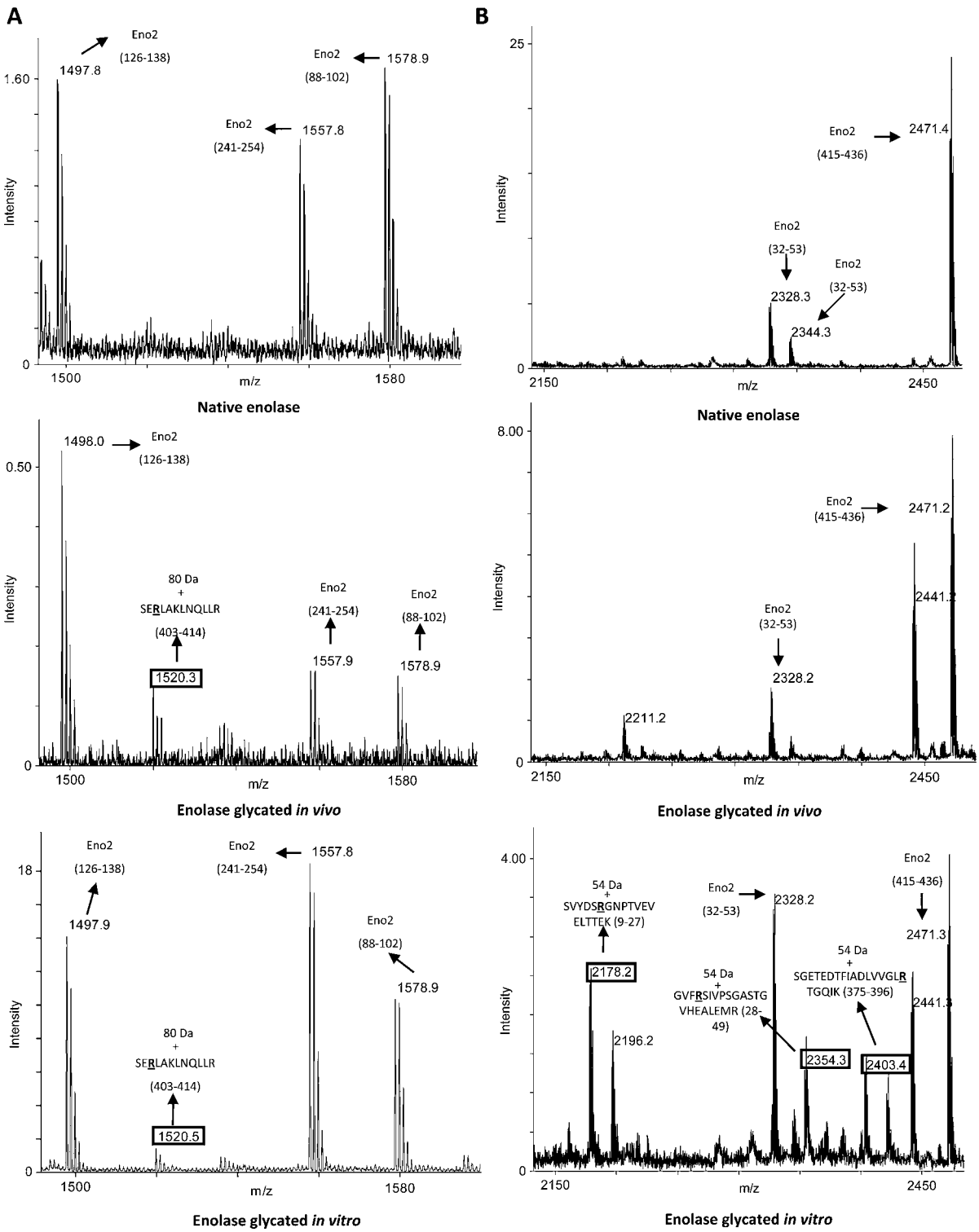

Figure 1 Chemical detection and molecular location of MAGEs in enolase

Glycated peptides show miscleavages associated with specific mass increments characteristics of a given MAGE [26]. This Figure shows sections of the MALDI–TOF mass spectrum where the appearance of new peptides with MAGEs in enolase glycated *in vivo* (**A**) and *in vitro* (**B**) are observed, in comparison with the native protein. The complete analysis of the MS data is presented in Tables 2 and 3.

strain, lacking the glyoxalase I gene and enzyme activity, hence with a higher intracellular methylglyoxal concentration than the reference strain. At the stationary phase of growth, glycation was observed [27]. Protein purity and identity were verified by SDS/PAGE and Western blot analysis with anti-yeast enolase antibody respectively. Protein identity was further confirmed by peptide mass fingerprint after in-gel trypsin digestion and MALDI–TOF analysis of the resulting peptide mixture (results not shown).

Table 1 Chemical identification and molecular localization of MAGEs in enolase by MALDI–TOF and MALDI–FTICR MS

Glycated residues are underlined and in bold. Argp, argpyrimidine.

Glycation	Observed mass (Da)	Theoretical peptide mass (Da)	Peptide sequence	Mass increase (Da)	MAGE	Glycated residue
In vitro	1269.67	1215.61	VYA**R**SVYDSR (5–14)	54.01	MG-H	Arg^{8}
	1310.63	1256.71	TGAPA**R**SE**R**LAK (397–408)	54.01	MG-H	Arg^{402} or Arg^{405}
	1520.14	1440.86	SE**R**LAKLNQLLR (403–414)	80.03	Argp	Arg^{405}
	1724.02	1669.92	LNQLL**R**IEEELGDK (409–422)	54.01	MG-H	Arg^{414}
	1741.92	1669.03	IATAIE**KK**AADALLLK (330–345)	72.02	CEL	Lys^{336} or Lys^{337}
	2010.19	1956.07	LGANAILGVSMAAA**R**AAAAEK (105–125)	54.01	MG-H	Arg^{119}
	2020.12	1965.99	TFAEAM**R**IGSEVYHNLK (178–194)	54.01	MG-H	Arg^{184}
	2178.18	2124.05	SVYDS**R**GNPTVEVELTTEK (9–27)	54.01	MG-H	Arg^{14}
	2354.32	2300.18	GVF**R**SIVPSGASTGVHEALEMR (28–49)	54.01	MG-H	Arg^{31}
	2403.42	2349.23	SGETEDTFIADLVVGL**R**TGQIK (375–396)	54.01	MG-H	Arg^{391}
	2635.57	2581.42	TAGIQIVADDLTVTNPA**R**IATAIEK (312–336)	54.01	MG-H	Arg^{329}
In vivo	1310.63	1256.71	TGAPA**R**SE**R**LAK (397–408)	54.01	MG-H	Arg^{402} or Arg^{405}
	1520.23	1440.86	SE**R**LAKLNQLLR (403–414)	80.03	Argp	Arg^{405}
	1741.90	1669.03	IATAIE**KK**AADALLLK (330–345)	72.02	CEL	Lys^{336} or Lys^{337}
	2252.20	2171.20	SKLGANAILGVSMAAA**R**AAAAEK (103–125)	54.01	MG-H	Arg^{119}
	1750.00*	1669.96	LNQLL**R**IEEELGDK (409–422)	80.03	Argp	Arg^{414}
	1654.83*	1600.84	AVSKVYA**R**SVYDSR (1–14)	54.01	MG-H	Arg^{8}

*Only observed by MALDI–FTICR-MS.

As previously shown, peptide mass fingerprint data contain hidden information regarding MAGE nature and location [26]. Since only lysine and arginine residues are modified, tryptic digestion of glycated proteins will produce peptides with at least one miscleavage associated with a defined mass increase corresponding to a specific MAGE (Figure 1). Proteins were also trypsin hydrolysed in solution to increase the sequence coverage and therefore improve MAGE identification. The resulting peptide mixtures were analysed by MALDI–TOF, ESI–FTICR-MS and MALDI–FTICR-MS. With the combination of these MS techniques, sequence coverage of approx. 70 % was obtained in all cases.

When enolase is glycated *in vitro*, ten out of 14 arginine residues are modified by methylglyoxal in the form of MG-H, whereas only one lysine residue, either Lys^{336} or Lys^{337}, is modified to CEL, as observed by MALDI–TOF and MALDI–FTICR (Table 1). These results are consistent with previous studies that point to MG-Hs as the most abundant modifications [45,46]. The analysis of the in-solution digest by ESI–FTICR-MS also revealed that some arginine residues even form different MAGE on different enolase molecules, such as Arg^{14} which may be modified as MG-H (observed mass of 2178.056 Da, corresponding to enolase peptide 9-27 with *m/z* of 2124.045 plus 54.011 Da of a MG-H modification) or as THP (observed mass of 2268.088 corresponding to the same enolase peptide 9-27 plus 144.042 Da of a THP modification) (Table 2). The same MAGE replacement was observed for Arg^{119} and Arg^{184} (Table 2). This molecular heterogeneity can be seen in a linear mode MALDI–TOF mass spectrum of *in vitro*-glycated enolase, showing a large mass increase and peak broadening compared with the molecular mass of native enolase (Figure 2). The formation of different MAGEs on the same amino acid residues hints that glycation is not specific *in vitro*. When enolase is glycated *in vivo*, only five arginine residues are found to be modified: Arg^{402} or Arg^{405}, Arg^{119} and Arg^{8} as MG-Hs and Arg^{405} and Arg^{414} as argpyrimidine (Table 1). Only one lysine residue was found as CEL. These modifications appear to be specific since no other MAGEs were found at these positions. In this case, the protein molecular mass increase is negligible, as observed by linear mode MALDI–TOF, indicating a lesser glycation extent, and no peak broadening or asymmetry, consistent with a homogeneous distribution of enolase molecular species (Figure 2).

To gain insights into the susceptibility of arginine residues towards methylglyoxal-derived glycation, its partial solvent exposure was calculated according to Gerstein [41] (Figure 3). For arginine modifications, no obvious relationship exists between the partial solvent exposure of amino groups and the susceptibility towards glycation. It is quite interesting to notice that arginine residues with reduced surface exposure of both side chain amino groups, such as arginine residues 119, 391, 405 and 414, are glycated. Meanwhile, the two arginine residues that show the highest surface exposure (Arg^{200} and Arg^{288}) were not found to be glycated. By contrast, solvent exposure appears to be a determinant factor for glycation of lysine residues since Lys^{336} and Lys^{337} show the highest solvent exposure of all lysine residues in enolase (results not shown).

Glycation effects on enolase folding, structure and enzyme activity

The effects of glycation on enolase structure were evaluated by far-UV CD spectroscopy after size-exclusion chromatography separation of each molecular form of enolase in solution (native, *in vivo*- and *in vitro*-glycated). Gel-filtration chromatograms clearly show two major peaks, one eluting at 20–25 min and the other at 35–40 min (Figure 4A). The first peak corresponds to the enzymatically active enolase dimer (90 kDa) with native secondary structure elements (Figures 4B and 4C). The second peak immunoreacts with an anti-yeast enolase antibody, but shows no CD signal and no enzyme activity, indicating the presence of unfolded, inactive enolase (Figures 4B–4D). Lack of absorption at 222 nm and 208 nm in the CD spectrum indicates a complete loss of regular secondary structural elements, consistent with the absence of enzyme activity. Similar results were obtained for folded and unfolded protein fractions of glycated enolase (results not shown). A comparison of the size-exclusion chromatograms show that, when glycation occurs, a higher fraction of unfolded inactive enolase is observed relative to the dimeric, folded enzyme (Figure 4A). For native enolase, the unfolded to folded area ratio is approx. one, whereas a 2-fold increase in this ratio is observed for *in vivo*-glycated enolase. When enolase is glycated

Table 2 Identification and localization of MAGEs in enolase glycated *in vitro* by methylglyoxal using ESI-FTICR-MS

Glycated residues are underlined and in bold. Noticeably, the same glycated amino acid residue appears with different chemical modifications.

Observed *m/z*	Charge	$[M+H]^+$	Theoretical peptide mass (Da)	Peptide sequence	Mass Increase (Da)	MAGE	Glycated residue
742.388	+3	2225.207	2171.196	SKLGANAILGVSMAAA**R**AAAAEK (103–125)	54.011	MG-H	Arg^{119}
1005.508	+2	2010.080	1956.070	LGANAILGVSMAAA**R**AAAAEK (105–125)	54.011	MG-H	Arg^{119}
772.375	+3	2315.239	2171.196	SKLGANAILGVSMAAA**R**AAAAEK (103–125)	144.042	THP	Arg^{119}
1089.478	+2	2178.056	2124.046	SVYDS**R**GNPTVEVELTTEK (9–27)	54.011	MG-H	Arg^{14}
726.67	+3	2178.056	2124.046	SVYDS**R**GNPTVEVELTTEK (9–27)	54.011	MG-H	Arg^{14}
879.771	+3	2637.315	2583.305	SVYDSRGNPTVEVELTTEKGVFR (9–31)	54.011	MG-H	Arg^{14}
756.68	+3	2268.088	2124.046	SVYDS**R**GNPTVEVELTTEK (9–27)	144.042	THP	Arg^{14}
1010.459	+2	2019.996	1965.985	TFAEAM**R**IGSEVYHNLK (178–194)	54.011	MG-H	Arg^{184}
1055.471	+2	2110.027	1965.985	TFAEAM**R**IGSEVYHNLK (178–194)	144.042	THP	Arg^{184}

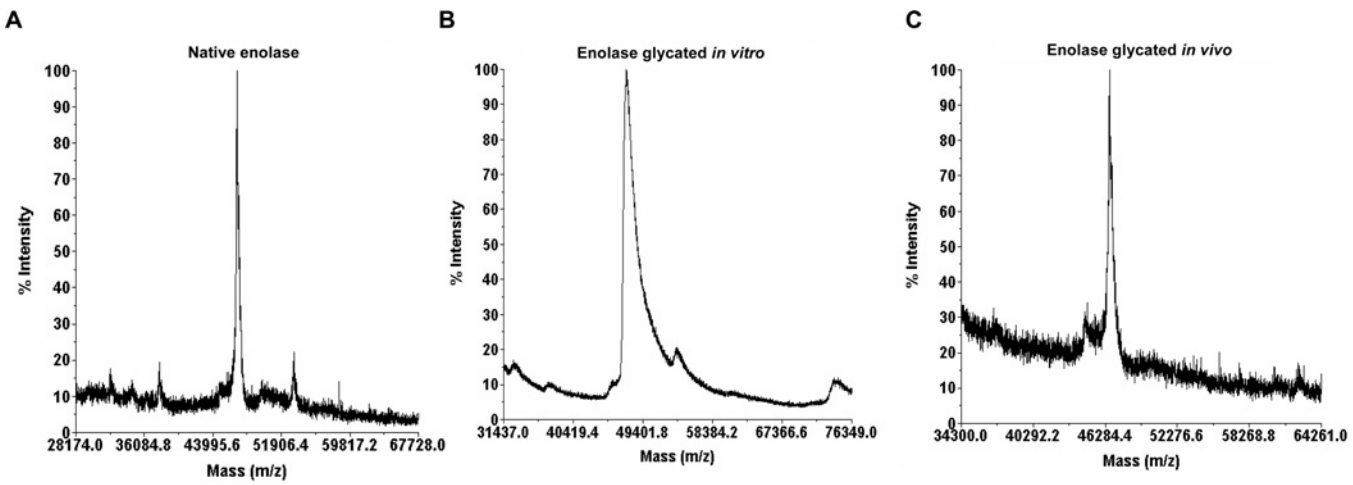

Figure 2 Analysis of intact protein mass by linear MALDI–TOF of native (A), *in vitro*-glycated (B) and *in vivo*-glycated (C) enolase

For all mass spectra, a peak with an *m/z* similar to theoretical yeast enolase 2 molecular mass (46782 Da) was obtained. With glycation *in vitro*, a broadening of the peak is observed indicating higher sample heterogeneity.

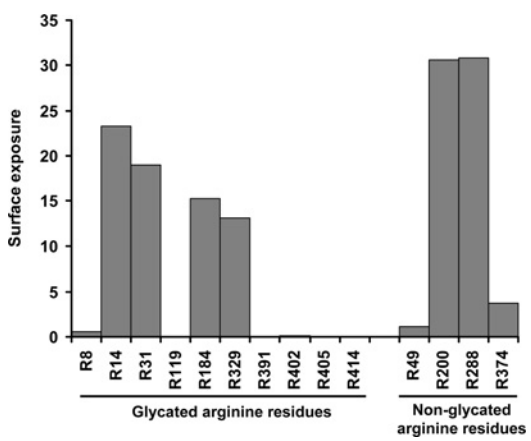

Figure 3 Surface exposure of arginine side chain in yeast enolase, calculated according to Gerstein [41]

Glycated and non-glycated arginine residues are shown.

in vitro, an even higher amount of unfolded enolase is observed, a 9-fold increase relative to the native enzyme.

If glycation promotes protein dissociation and unfolding, then both protein fractions should be glycated. To confirm this hypothesis, these fractions were separated by size-exclusion chromatography, analysed by reversed-phase HPLC with fluorescence detection at $\lambda_{ex.320}\lambda_{em.385}$ (characteristic of argpyrimidine) and by Western blot analysis using an anti-MAGE antibody. Indeed, both protein fractions derived from enolase glycated *in vivo* and *in vitro* contain argpyrimidine and other MAGEs (Figure 4E). These results clearly show that enolase glycation causes protein unfolding and since glycation is an irreversible process, unfolded protein may not be refolded back to the active enzyme form. The effect is far more severe when the protein is glycated *in vitro*.

Once the different enolase molecular species were separated by size-exclusion chromatography, samples were analysed by far-UV CD spectroscopy. Striking differences were observed, particularly within the regions of 195 nm, 208 nm and 222 nm (Figure 5A). In native enolase, the α-helical content was 40 %, β-sheet was 20 %, 21 % of turns and 19 % of unordered structure (Table 3). These values are in agreement with the values of 37.6 % for α-helix, 21 % of β-sheet, 26 % of turns and 15.4 % unordered structures obtained by Fourier transformed IR spectroscopy [32]. X-ray crystallography analysis of yeast enolase, estimated an α-helical content of 37.3 % and 17.2 % of β-sheet [47]. *In vivo*-glycated enolase shows little to no secondary structure loss. However, a redistribution of secondary structure elements is evident, with an increase in unordered structure from 19 % to 25 %, a reduction in the α-helical content from 40 % to 35 %, whereas β-sheet content

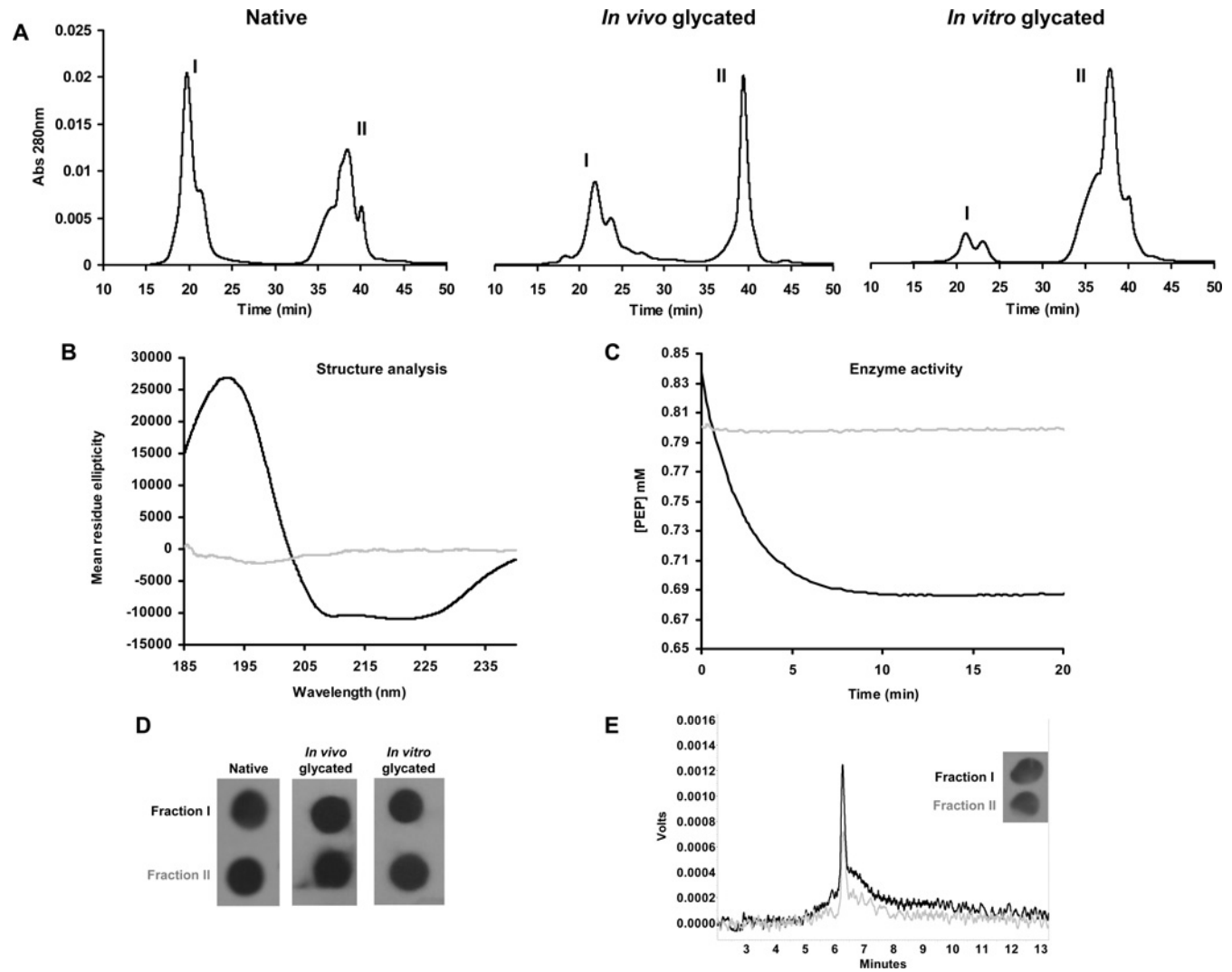

Figure 4 Characterization of the different enolase species

(**A**) Size-exclusion chromatography of native, glycated *in vivo* and glycated *in vitro* enolase, showing the presence of two major protein fractions (marked as fractions I and II). (**B**) Far-UV CD spectra of fraction I (black) and fraction II (light grey) collected from gel filtration of native enolase. Contrary to fraction I, no CD signal was observed in fraction II, showing a complete loss of secondary structure elements. (**C**) Enolase activity assays of fraction I (black) and II (light grey). Consistent with the lack of secondary structure, no enzyme activity was detected in fraction II. (**D**) Dot-blot analysis of both fractions with an anti-yeast enolase antibody, with positive results. (**E**) Glycation analysis by HPLC and dot-blot analysis of fraction I (black) and fraction II (light grey) from enolase glycated *in vivo*. Both fractions show a fluorescent peak at approx. 6 min at wavelengths characteristic of argpyrimidine ($\lambda_{ex.320}/\lambda_{em.385}$) indicating that both fractions are glycated. The positive signal obtained by dot-blot analysis with an anti-MAGE antibody also indicates that both fractions are glycated.

remains unchanged (Table 3). When enolase is glycated *in vitro*, a distinct scenario emerges. There is a much higher loss of α-helix content, from 40 % to 17 %, and a large increase in β-sheet, from 20 % to 32 %, compared with *in vivo*-glycated enolase (Table 3). Unordered structure elements also increase, from 19 % to 32 %.

To evaluate the glycation effects on the structural stability of enolase, thermal denaturation of the native, *in vivo*- and *in vitro*-glycated enolase was monitored by CD spectroscopy. Glycation shifts the thermal denaturation curve of enolase to higher temperatures, indicating an increased resistance to thermal unfolding (Figure 5B). In fact, the T_m for native enolase is 53.6 °C, whereas *in vivo*-glycated enolase shows a T_m of 58.6 °C and the *in vitro*-glycated enolase an even higher T_m of 61.4 °C. Enolase thermal denaturation is an irreversible process, as confirmed by protein aggregation and lack of secondary structure analysed by CD when the temperature was returned to 25 °C (results not shown), hence the determination of thermodynamic parameters could not be performed.

Table 3 Secondary structure elements for native, *in vivo*- and *in vitro*-glycated enolase, obtained by CD spectra deconvolution with the CDSSTR algorithm (Dichroweb; http://www.cryst.bbk.ac.uk/cdweb/html/home.html)

NRMSD, normalized root mean square deviation.

Structural elements	α-Helix	β-Sheet	β-Turns	Unordered structure	NRMSD
Native	0.40	0.20	0.21	0.19	0.011
Glycated *in vivo*	0.35	0.20	0.20	0.25	0.017
Glycated *in vitro*	0.17	0.32	0.19	0.32	0.026

Secondary structure changes are associated with protein function modifications. Therefore glycation-induced conformational

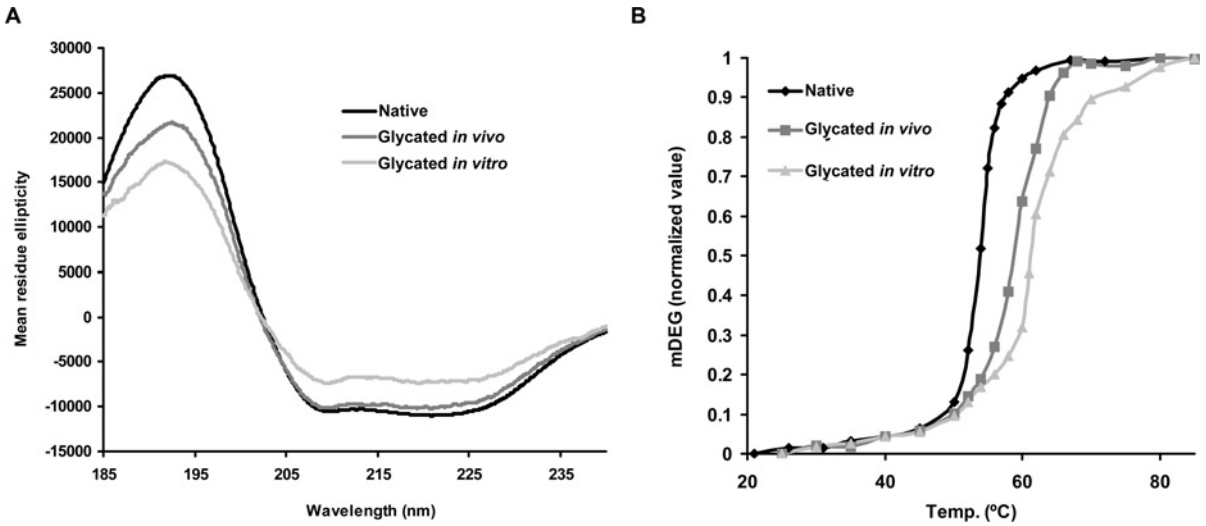

Figure 5 Enolase structure and stability

(**A**) Far-UV CD spectra of native, *in vivo*-glycated and *in vitro*-glycated enolase between 185 and 240 nm. (**B**) Thermal denaturation of native, *in vivo*- and *in vitro*-glycated enolase. Upon glycation, a shift towards higher melting temperatures is observed.

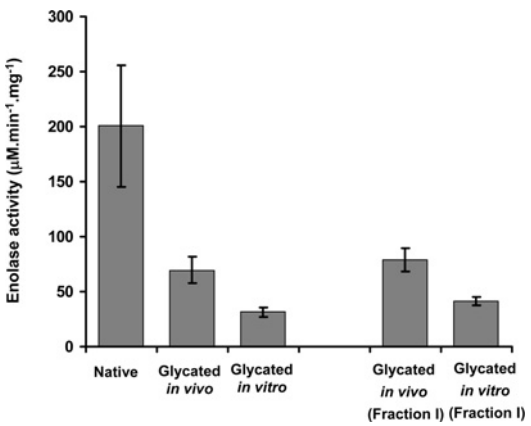

Figure 6 Glycation effects on enolase activity

Enolase activity was determined by the consumption of phosphoenolpyruvate, as described in the Experimental section. Glycation induces a considerable activity loss. Fraction I contains folded active enolase. Values shown are averages from three independent activity assays ± S.D.

changes are likely to have pronounced effects on enolase activity. Indeed, we observed a marked decrease in enolase activity upon glycation (Figure 6). *In vivo*-glycated enolase shows a 65 % activity loss compared with native enolase. When enolase is glycated *in vitro*, an even more severe activity loss is observed (84 %). As glycation causes enolase denaturation with a consequent enzyme inactivation, it could be argued that the loss of enzyme-specific activity may be solely explained by the higher amount of unfolded inactive protein in the sample. This implies that, if the activity of glycated folded enolase remained the same, the specific activity would decrease. To investigate this hypothesis, folded and unfolded fractions from *in vivo*- and *in vitro*-glycated enolase were separated by size-exclusion chromatography and enzyme activity was determined for each individual fraction (fraction I being folded active and glycated enolase, whereas fraction II is unfolded glycated enolase). In both cases, no enolase activity was detected in fraction II, consistent with the lack of secondary structure. In fraction I, enolase activity was detected, albeit the specific activity was again much lower than that of the native enzyme (Figure 6).

DISCUSSION

Arginine residues have a probability of approx. 20 % of being located in ligand- and substrate-binding sites of proteins [48]. Hence, methylglyoxal-derived arginine glycation is expected to have significant effects on protein structure and function, being related to several human pathologies [3,4,8,10,11]. Therefore this post-translational modification has been the subject of intensive research, where *in vitro*-glycation of clinically relevant and model proteins was investigated [22,23,45]. The major drawback of this approach lies on the dramatic differences between glycation conditions *in vitro* and *in vivo*. *In vitro*, non-physiological concentrations of glycation agents are used, from millimolar to molar concentrations [21–24]. Additionally, protein interactions are not taken into account. Also, protein turnover and the action of molecular chaperones, some of which are activated upon glycation by methylglyoxal [19,20,26], is absent. These differences highlight the importance of investigating protein glycation mechanisms and their biochemical effects *in vivo*. Our previous studies validated yeast as a eukaryotic cell model to investigate protein glycation *in vivo* [26,27]. Enolase, the major glycation target, shows glycation-dependent activity loss [26], providing an important model for studying glycation effects *in vivo*.

In agreement with our hypothesis that protein glycation is different *in vivo* and *in vitro*, MS analysis indicates that enolase glycation *in vivo* is site-specific whereby only a few amino acid residues are consistently modified with the same MAGEs. By contrast, glycation *in vitro* is a heterogeneous process, resulting in the formation of a complex population of enolase molecules with different glycation profiles. *In vitro*, different MAGEs may be present at the same arginine residue, in different protein molecules. Glycation specificity is not related to the partial solvent exposure of arginine residues (Figure 3). We previously suggested that the arginine-rich deep crevice in enolase protein structure, accessible to the solvent and located at the dimer interface, may be a favourable hotspot for the occurrence of glycation [26]. Several glycated arginine residues identified after *in vitro*-glycation and

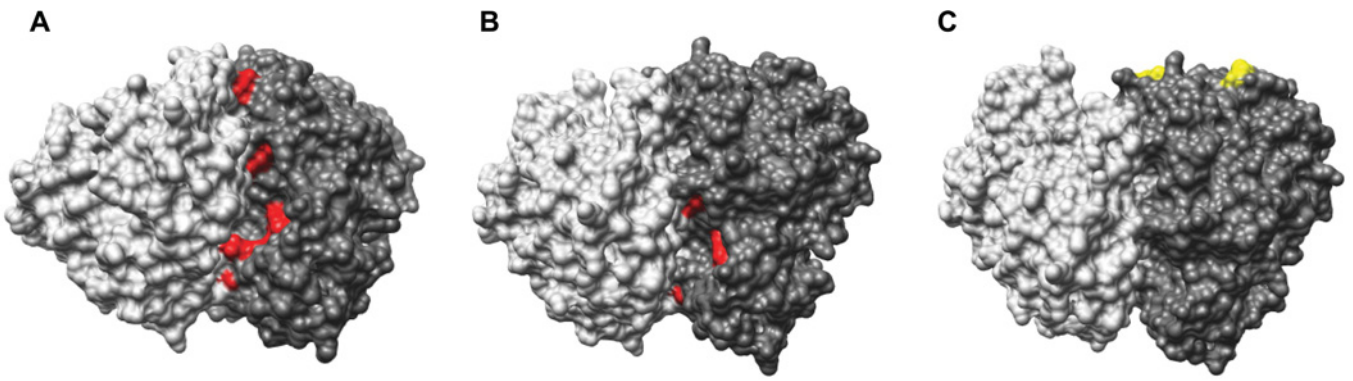

Figure 7 Surface landscape of dimeric yeast enolase, showing the glycated (red) and non-glycated (yellow) arginine residues

For greater clarity, the surface of one of the subunits is shown in light grey. (**A**) Enolase glycated *in vitro* showing glycated arginine residue in a cleft at the dimer interface. (**B**) *In vivo*-glycated enolase showing four out of five glycated arginine residues in the cleft between the two monomers. (**C**) Enolase structure showing the highest solvent exposed arginine residues Arg^{200} and Arg^{288} that were not glycated. Interestingly, these arginine residues are not located at the dimer interface.

almost all glycated arginines *in vivo* are located in this cleft (Figures 7A and 7B). Interestingly, glycation was not detected in the two most exposed arginine residues (Arg^{200} and Arg^{288}), outside the cleft (Figure 7C).

In vivo-glycated enolase shows an increase of unordered structure. α-Helical content decreases and T_m increases with glycation, suggesting that glycated enolase may exist in a more compact and rigid conformation. When enolase was glycated *in vitro*, besides an enhanced increase in unordered structure and a decrease in α-helix, a marked gain of β-sheet was also observed. The T_m increase is more pronounced, consistent with an even more rigid structure, probably due to higher β-sheet content.

Glycation also leads to enolase unfolding. This is in agreement with our previous model of glycation-induced enolase inactivation in which the glycation of the critical arginine residue 414 disrupted an ionic pair formed with glutamate residue 20, essential for dimer stability [26]. A modification of Arg^{414} was observed in the present study, both as a consequence of *in vivo*- and *in vitro*-glycation. When enolase is glycated *in vitro*, unfolding is much more pronounced. This can be due to the higher glycation extent or because the molecular chaperone pathway which is activated by glycation *in vivo* is absent from a test tube [19,26]. The observed changes in protein structure and stability are related to the glycation-dependent activity loss, 65 % inactivation *in vivo* and 85 % activity loss *in vitro*.

The results of the present study reveal important differences between glycation *in vivo* and *in vitro* in the conditions used, which may be related to diverse glycation specificities. This observation highlights the importance of investigating protein glycation *in vivo* in a model system such as yeast, already validated in the research of amyloidotic neurodegenerative diseases [49].

We thank Dr H. M. Park for the gift of the anti-yeast-enolase polyclonal antibody and Dr Ram Nagaraj for the gift of the anti-MAGE antibody. We wish to acknowledge Dr Ana Varela Coelho for providing data from the Laboratório de espectrometria de massa at the Instituto de Tecnologia Química e Biológica, Universidade Nova de Lisboa, Oeiras, Portugal. Work was supported by grants SFRH/BD/13884/2003 (R. A. G.), SFRH/BPD/28345/2006 (M. S. S.) and SFRH/BD/23604/2005 (L. M. A. O.) from the Fundação para a Ciência e a Tecnologia, Ministério da Ciência e Tecnologia, Portugal.

REFERENCES

1 Westwood, M. E. and Thornalley, P. J. (1997) Glycation and advanced glycation endproducts, In The Glycation Hypothesis of Atherosclerosis (Colaco, C., ed.). pp. 57–87, Landes Bioscience, Austin, TX

2 Grillo, M. A. and Colombatto, S. (2008) Advanced glycation end-products (AGEs): involvement in aging and in neurodegenerative diseases. Amino Acids **35**, 29–36

3 Brownlee, M. (1995) Advanced protein glycosylation in diabetes and aging. Annu. Rev. Med. **46**, 223–234

4 Miyata, T., Ueda, Y., Saito, A. and Kurokawa, K. (2000) 'Carbonyl stress' and dialysis-related amyloidosis. Nephrol. Dial. Transplant. **15**, (Suppl. 1), 25–28

5 Kume, S., Takeya, M., Mori, T., Araki, N., Suzuki, H., Horiuchi, S., Kodama, T., Miyauchi, Y. and Takahashi, K. (1995) Immunohistochemical and ultrastructural detection of advanced glycation end products in atherosclerotic lesions of human aorta with a novel specific monoclonal antibody. Am. J. Pathol. **147**, 654–667

6 Miyata, T., Inagi, R., Iida, Y., Sato, M., Yamada, N., Oda, O., Maeda, K. and Seo, H. (1994) Involvement of β2-microglobulin modified with advanced glycation end products in the pathogenesis of hemodialysis-associated amyloidosis. Induction of human monocyte chemotaxis and macrophage secretion of tumor necrosis factor-α and interleukin-1. J. Clin. Invest. **93**, 521–528

7 Shibata, N., Hirano, A., Hedley-Whyte, E. T., Dal Canto, M. C., Nagai, R., Uchida, K., Horiuchi, S., Kawaguchi, M., Yamamoto, T. and Kobayashi, M. (2002) Selective formation of certain advanced glycation end products in spinal cord astrocytes of humans and mice with superoxide dismutase-1 mutation. Acta Neuropathol. **104**, 171–178

8 Vitek, M. P., Bhattacharya, K., Glendening, J. M., Stopa, E., Vlassara, H., Bucala, R., Manogue, K. and Cerami, A. (1994) Advanced glycation end products contribute to amyloidosis in Alzheimer disease. Proc. Natl. Acad. Sci. U.S.A. **91**, 4766–4770

9 Yan, S. D., Chen, X., Schmidt, A. M., Brett, J., Godman, G., Zou, Y. S., Scott, C. W., Caputo, C., Frappier, T. and Smith, M. A. (1994) Glycated tau protein in Alzheimer disease: a mechanism for induction of oxidant stress. Proc. Natl. Acad. Sci. U.S.A. **91**, 7787–7791

10 Castellani, R., Smith, M. A., Richey, P. L. and Perry, G. (1996) Glycoxidation and oxidative stress in Parkinson disease and diffuse Lewy body disease. Brain Res. **737**, 195–200

11 Gomes, R., Sousa Silva, M., Quintas, A., Cordeiro, C., Freire, A., Pereira, P., Martins, A., Monteiro, E., Barroso, E. and Ponces Freire, A. (2005) Argpyrimidine, a methylglyoxal-derived advanced glycation end-product in familial amyloidotic polyneuropathy. Biochem. J. **385**, 339–345

12 Baynes, J. W. and Thorpe, S. R. (1999) Role of oxidative stress in diabetic complications: a new perspective on an old paradigm. Diabetes **48**, 1–9

13 Richard, J. P. (1984) Acid–base catalysis of the elimination and isomerization-reactions of triose phosphates. J. Am. Chem. Soc. **106**, 4926–4936

14 Richard, J. P. (1993) Mechanism for the formation of methylglyoxal from triosephosphates. Biochem. Soc. Trans. **21**, 549–553

15 Thornalley, P. J. (1996) Pharmacology of methylglyoxal: formation, modification of proteins and nucleic acids, and enzymatic detoxification-a role in pathogenesis and antiproliferative chemotherapy. Gen. Pharmacol. **27**, 565–573

16 Kilhovd, B. K., Giardino, I., Torjesen, P. A., Birkeland, K. I., Berg, T. J., Thornalley, P. J., Brownlee, M. and Hanssen, K. F. (2003) Increased serum levels of the specific AGE-compound methylglyoxal-derived hydroimidazolone in patients with type 2 diabetes. Metab. Clin. Exp. **52**, 163–167

16a Speer, O., Morkunaite-Haimi, S., Liobikas, J., Franck, M., Hensbo, L., Linder, M. D., Kinnunen, P. K., Wallimann, T. and Eriksson, O. (2003) Rapid suppression of mitochondrial permeability transition by methylglyoxal. Role of reversible arginine modification. J. Biol. Chem. **278**, 34757–34763

16b Pedchenko, V. K., Chetyrkin, S. V., Chuang, P., Ham, A. J., Saleem, M. A., Mathieson, P. W., Hudson, B. G. and Voziyan, P. A. (2005) Mechanism of perturbation of integrin-mediated cell-matrix interactions by reactive carbonyl compounds and its implication for pathogenesis of diabetic nephropathy. Diabetes **54**, 2952–2960
16c Portero-Otín, M., Pamplona, R., Bellmunt, M. J., Ruiz, M. C., Prat, J., Salvayre, R. and Nègre-Salvayre, A. (2002) Advanced glycation end product precursors impair epidermal growth factor receptor signaling. Diabetes **51**, 1535–1542
17 Sakamoto, H., Mashima, T., Yamamoto, K. and Tsuruo, T. (2002) Modulation of heat-shock protein 27 (Hsp27) anti-apoptotic activity by methylglyoxal modification. J. Biol. Chem. **277**, 45770–45775
18 Gomes, R. A., Miranda, H. V., Sousa Silva, M., Graca, G., Coelho, A. V., do Nascimento Ferreira, A. E., Cordeiro, C. and Freire, A. P. (2008) Protein glycation and methylglyoxal metabolism in yeast: finding peptide needles in protein haystacks. FEMS Yeast Res. **8**, 174–181
19 Nagaraj, R. H., Oya-Ito, T., Padayatti, P. S., Kumar, R., Mehta, S., West, K., Levison, B., Sun, J., Crabb, J. W. and Padival, A. K. (2003) Enhancement of chaperone function of α-crystallin by methylglyoxal modification. Biochemistry **42**, 10746–10755
20 Oya-Ito, T., Liu, B. F. and Nagaraj, R. H. (2006) Effect of methylglyoxal modification and phosphorylation on the chaperone and anti-apoptotic properties of heat shock protein 27. J. Cell Biochem. **99**, 279–291
21 Bakhti, M., Habibi-Rezaei, M., Moosavi-Movahedi, A. A. and Khazaei, M. R. (2007) Consequential alterations in haemoglobin structure upon glycation with fructose: prevention by acetylsalicylic acid. J. Biochem. (Tokyo) **141**, 827–833
22 Bouma, B., Kroon-Batenburg, L. M., Wu, Y. P., Brunjes, B., Posthuma, G., Kranenburg, O., de Groot, P. G., Voest, E. E. and Gebbink, M. F. (2003) Glycation induces formation of amyloid cross-β structure in albumin. J. Biol. Chem. **278**, 41810–41819
23 Luthra, M. and Balasubramanian, D. (1993) Nonenzymatic glycation alters protein structure and stability. A study of two eye lens crystallins. J. Biol. Chem. **268**, 18119–18127
24 Seidler, N. W. and Kowalewski, C. (2003) Methylglyoxal-induced glycation affects protein topography. Arch. Biochem. Biophys. **410**, 149–154
25 Srere, P. A. (1987) Complexes of sequencial metabolic enzymes. Annu. Rev. Biochem. **56**, 89–124
26 Gomes, R. A., Miranda, H. V., Silva, M. S., Graca, G., Coelho, A. V., Ferreira, A. E., Cordeiro, C. and Freire, A. P. (2006) Yeast protein glycation *in vivo* by methylglyoxal. Molecular modification of glycolytic enzymes and heat shock proteins. FEBS J. **273**, 5273–5287
27 Gomes, R. A., Sousa Silva, M., Vicente Miranda, H., Ferreira, A. E., Cordeiro, C. A. and Freire, A. P. (2005) Protein glycation in *Saccharomyces cerevisiae*. Argpyrimidine formation and methylglyoxal catabolism. FEBS J. **272**, 4521–4531
28 Kellum, M. W., Oray, B. and Norton, S. J. (1978) A convenient quantitative synthesis of methylglyoxal for glyoxalase I assays. Anal. Biochem. **85**, 586–590
29 McLellan, A. C., Phillips, S. A. and Thornalley, P. J. (1992) The assay of methylglyoxal in biological systems by derivatization with 1,2-diamino-4,5-dimethoxybenzene. Anal. Biochem. **206**, 17–23
30 Racker, E. (1951) The mechanism of action of glyoxalase. J. Biol. Chem. **190**, 685–696
31 Kustrzeba-Wojcicka, I. and Golczak, M. (2000) Enolase from *Candida albicans*-purification and characterization. Comp. Biochem. Physiol. B Biochem. Mol. Biol. **126**, 109–120
32 Huang, P. and Dong, A. (2003) Thermal, chemical and chemothermal denaturation of yeast enolase. Spectroscopy **17**, 453–467
33 Pandey, A., Andersen, J. S. and Mann, M. (2000) Use of mass spectrometry to study signaling pathways. Science STKE **2000**, PL1
34 Gobom, J., Nordhoff, E., Mirgorodskaya, E., Ekman, R. and Roepstorff, P. (1999) Sample purification and preparation technique based on nano-scale reversed-phase columns for the sensitive analysis of complex peptide mixtures by matrix-assisted laser desorption/ionization mass spectrometry. J. Mass Spectrom. **34**, 105–116
35 Olsen, J. V. and Mann, M. (2004) Improved peptide identification in proteomics by two consecutive stages of mass spectrometric fragmentation. Proc. Natl. Acad. Sci. U.S.A. **101**, 13417–13422
36 Johnson, W. C. (1999) Analyzing protein circular dichroism spectra for accurate secondary structures. Proteins **35**, 307–312
37 Lobley, A., Whitmore, L. and Wallace, B. A. (2002) DICHROWEB: an interactive website for the analysis of protein secondary structure from circular dichroism spectra. Bioinformatics **18**, 211–212
38 Whitmore, L. and Wallace, B. A. (2004) DICHROWEB, an online server for protein secondary structure analyses from circular dichroism spectroscopic data. Nucleic Acids Res. **32**, W668–W673
39 Pace, C. N., Shirley, B. A. and Thomson, J. A. (1990) Measuring the conformational stability of a protein, In Protein Structure: a Practical Approach (Creighton, T.E.E., ed.). pp. 311–330, Oxford University Press, Oxford, U.K.
40 Pettersen, E. F., Goddard, T. D., Huang, C. C., Couch, G. S., Greenblatt, D. M., Meng, E. C. and Ferrin, T. E. (2004) UCSF Chimera: a visualization system for exploratory research and analysis. J. Comput. Chem. **25**, 1605–1612
41 Gerstein, M. (1992) A resolution-sensitive procedure for comparing protein surfaces and its application to the comparison of antigen-combining sites. Acta Crystallogr. Sect. A Found. Crystallogr. **48**, 271–276
42 Kang, J. H. (2003) Modification and inactivation of human Cu,Zn-superoxide dismutase by methylglyoxal. Mol. Cells **15**, 194–199
43 Shipanova, I. N., Glomb, M. A. and Nagaraj, R. H. (1997) Protein modification by methylglyoxal: chemical nature and synthetic mechanism of a major fluorescent adduct. Arch. Biochem. Biophys. **344**, 29–36
44 Ahmed, M. U., Brinkmann Frye, E., Degenhardt, T. P., Thorpe, S. R. and Baynes, J. W. (1997) N-ε-(carboxyethyl)lysine, a product of the chemical modification of proteins by methylglyoxal, increases with age in human lens proteins. Biochem. J. **324**, 565–570
45 Ahmed, N., Dobler, D., Dean, M. and Thornalley, P. J. (2005) Peptide mapping identifies hotspot site of modification in human serum albumin by methylglyoxal involved in ligand binding and esterase activity. J. Biol. Chem. **280**, 5724–5732
46 Ahmed, N., Thornalley, P. J., Dawczynski, J., Franke, S., Strobel, J., Stein, G. and Haik, G. M. (2003) Methylglyoxal-derived hydroimidazolone advanced glycation end-products of human lens proteins. Invest. Ophthalmol. Vis. Sci. **44**, 5287–5292
47 Stec, B. and Lebioda, L. (1990) Refined structure of yeast apo-enolase at 2.25 Å resolution. J. Mol. Biol. **211**, 235–248
48 Gallet, X., Charloteaux, B., Thomas, A. and Brasseur, R. (2000) A fast method to predict protein interaction sites from sequences. J. Mol. Biol. **302**, 917–926
49 Outeiro, T. F. and Lindquist, S. (2003) Yeast cells provide insight into α-synuclein biology and pathobiology. Science. **302**, 1772–1775

Received 25 March 2008/18 July 2008; accepted 23 July 2008
Published as BJ Immediate Publication 23 July 2008, doi:10.1042/BJ20080632